Skin Lesion Image Segmentation Using a Color Genetic Algorithm

Alessia Amelio
National Research Council of Italy (CNR)
Inst. for High Perf. Comp. and Networking (ICAR)
Via P. Bucci 41C, 87036 Rende(CS), Italy
amelio@icar.cnr.it

Clara Pizzuti
National Research Council of Italy (CNR)
Inst. for High Perf. Comp. and Networking (ICAR)
Via P. Bucci 41C, 87036 Rende(CS), Italy
pizzuti@icar.cnr.it

ABSTRACT

The development of computer-aided diagnosis systems for skin cancer detection has attracted a lot of interest in the research community. In particular, the availability of an accurate automatic segmentation tool for detecting skin lesions from background skin is of primary importance for the overall diagnosis system. In this paper we investigate the capability of a color image segmentation method based on Genetic Algorithms in discriminating skin lesions. Experimental results show that the segmentation approach is able to detect lesion borders quite accurately, thus coupled with a merging technique of the surrounding region could reveal a promising method for isolating skin tumor.

Categories and Subject Descriptors

H.2.8 [**Database Managment**]: Database Applications —*Data Mining*; I.4.6 [**Image Processing and Computer Vision**]: Segmentation; I.5.3 [**Pattern Recognition**]: Clustering

General Terms

Algorithms

Keywords

Image segmentation, Genetic algorithms, Medical images

1. INTRODUCTION

The application of automatic computerized image analysis methods for skin lesion detection is an active research area that can give a valid help in early diagnosing skin cancer [4]. Computer-assisted diagnosis of skin lesions is a valid support for clinicians because, often, visual inspection is not adequate for early detection, which is decisive for increasing survival rate. It consists of five general steps [10] : image acquisition, preprocessing, segmentation, feature extraction, and classification. After a digital image is acquired, it is preprocessed to improve its quality by eliminating noise or artifacts present on the image, such as hairs, normalizing pixel intensity, removing reflection. The next step amounts to image segmentation. This step is crucial for automated diagnosis since the detection of accurate borders of the skin lesion affects the accuracy of subsequent phases. After that, the main features of the lesion are extracted to feed into a classifier system that must decide whether the lesion is either malignant or benign.

A segmentation technique should trace the lesion borders as much accurately as possible and should avoid oversegmentation. Because of the importance of correct border identification, a high number of segmentation techniques have been developed using different approaches such as fuzzy logic based thresholding [22], clustering [15, 12, 18, 24, 23], neural networks [6, 17], supervised learning [20], active contour [23], evolutionary computation [21]. However, it is worth to note that there is no a general technique suitable for all the kinds of applications.

In this paper we investigate the capability of a color image segmentation technique, based on Genetic Algorithms, in discriminating skin lesion. The method, named *C-GeNCut* (*Color Genetic Normalized Cut*) and presented in [1], represents an image as a weighted undirected graph, where nodes correspond to pixels, and edges connect similar pixels. Similarity between two pixels is computed by taking into account brightness, color and texture content. The algorithm has been tested on ten skin images presenting different types of tumor, and compared with the algorithm of Maji et al. [13].

The paper is organized as follows. The next section gives a description of the method used. Section 3 presents the result of the experiments on the skin lesion images, Section 4 concludes the paper and outlines future research directions.

2. METHODOLOGY

In this section we review the main concepts of the method *C-GeNCut* [1].

An image R is represented as a weighted undirected graph $G = (V, E, w)$, whose nodes V correspond to image pixels, and an edge $(i, j) \in E$ connects two pixels i and j if they satisfy some property suitably defined that takes into account both pixel characteristics and spatial distance. $w : E \rightarrow \mathcal{R}$ is a function that assigns a weight to graph edges. A weight $w(i, j)$ corresponds to the likelihood that pixels i and j are in the same image region and represents a similarity value between i and j. The higher the value of $w(i, j)$, the more

GECCO'13 Companion, July 6–10, 2013, Amsterdam, The Netherlands.

likely the two pixels are within the same region. Let W denote the adjacency weight matrix of the graph G. A generic element W_{ij} contains the weight $w(i,j)$ if nodes i and j are connected, zero otherwise.

The computation of weights is performed by using the *Intervening Contour* cue [11, 5, 8, 7], based on the multispectral Pb detector as defined in [2].

In this framework, given a generic pixel, the value of the multiscale Pb detector at that pixel is considered. If the maximum value along a straight line connecting the two pixels i and j in the image plan is large, then a deep change in brightness, color and texture and, consequently, an intervening contour is present, indicating that the two pixels don't belong to the same segment. On the other hand, if the value of the multiscale Pb detector is sufficiently weak, the affinity between the two pixels will be very high. More formally, the weight $w(i,j)$ between the pixels i and j is computed as:

$$w(i,j) = \begin{cases} e^{-max_{p \in line(i,j)}\{mPb(p)\}/\rho} & \text{if } ||X(i) - X(j)||_2 < r, i \neq j \\ 0 & \text{otherwise.} \end{cases}$$

where *line(i,j)* is a straight line between i and j, *X(i)* is the spatial location of the pixel i, r is a distance threshold and ρ is a constant.

Multiscale Pb detector is based on the Pb detector function $Pb(x,y,\theta)$, which is obtained by evaluating the difference in local image brightness, color and texture channels.

Specifically, input image is transformed into four distinct channels. The first three channels are those of the CIE Lab colorspace, taking into account brightness and color, while the last channel is related to the image texture content. For each image channel, an oriented gradient signal is computed, $G(x,y,\theta)$, at position (x,y), by placing a circular disc centered at location (x,y), splitting it into two half-discs by a diameter at angle θ, and finally computing the χ^2 distance between the intensity histograms of the two half-discs. Furthermore, gradients at three scales $[\sigma/2, \sigma, 2\sigma]$ are considered for each channel, in order to detect fine and coarse image features.

The Pb detector processes the channels separately and then combines the oriented gradient signals obtained from the different channels at multiple scales into a single multiscale oriented signal:

$$mPb(x,y,\theta) = \sum_s \sum_i \alpha_{i,s} G_{i,\sigma(i,s)}(x,y,\theta)$$

where s represents the scales index, i the feature channels index (brightness, color a, color b and texture). The oriented gradient signal is $G_{i,\sigma(i,s)}(x,y,\theta)$ in channel i where the radius of the disc is $\sigma(i,s)$. The parameters $\alpha_{i,s}$ weight the contribution of each gradient signal. The angle θ defining the orientation, takes eight different values in the interval $[0,\pi)$. The final value of the multispectral Pb detector is the maximum response over the eight orientations:

$$mPb(x,y) = max_\theta\{mPb(x,y,\theta)\}.$$

2.1 Genetic Representation and Operators

The representation of individuals is the locus-based adjacency representation proposed in [16]. In this graph-based representation an individual of the population consists of N genes $g_1, \ldots, g_N$ and each gene can assume allele values j in the range $\{1, \ldots, N\}$. Genes and alleles represent nodes of the graph $G = (V, E, w)$ modelling an image, and a value j assigned to the ith gene is interpreted as a link between the pixels i and j. The initialization process assigns to each node i one of its neighbors j, and the kind of crossover operator adopted is uniform crossover. The mutation operator randomly assigns to each node i one of its neighbors. For both initialization and mutation, the determination of the neighbors of each node takes into account not only the spatial closeness but also the pixel affinity. More in details, given a generic node i in the graph, let $w^h_{max} = \{w^1, \ldots, w^h \mid w^1 \geq, \ldots, \geq w^h\}$ be the first h highest weights of row i in the weight adjacency matrix W.

The h nearest neighbors of i, denoted as nn^h_i, are then defined as $nn^h_i = \{j \mid w(i,j) \in w^h_{max}\}$. nn^h_i is thus the set of those pixels that are no more than r pixels apart from i, and that have maximum similarity with i. The kind of crossover adopted is uniform crossover.

2.2 Fitness Function

The fitness function is an extension of the concept of normalized cut of Shi and Malik [19]. Let $G = (V, E, w)$ be the graph representing an image, W its adjacency matrix, and $P = \{R_1, \ldots, R_k\}$ a partition of G in k clusters.

For a generic cluster $R \in P$, let

$$c_r = \sum_{i \in R, j \notin R} W_{ij} \qquad m_r = \sum_{i \in R, j \in R} W_{ij} \qquad m = \sum_{i \in V, j \in V} W_{ij}$$

be respectively the sum of weights of edges on the boundary of R, the sum of weights of edges inside R, and the total graph weight sum. The *weighted normalized cut WNCut* measures for each cluster in P the fraction of total edge weight connections to all the nodes in the graph

$$WNCut = \sum_{r=1}^{k} \frac{c_r}{m_r + c_r} + \frac{c_r}{(m - m_r) + c_r}$$

Because of the adopted affinity measure w, more uniform regions can be obtained with low cut values between the subgraphs representing the regions and the rest of the graph. This implies that low values of $WNcut$ are preferred.

3. EXPERIMENTAL RESULTS

In this section we present the results of *C-GeNCut* on six skin lesion images representing different melanoma (Figures (1-6)) and on four images depicting other kinds of skin tumors different from melanoma (Figures (7-10)), and evaluate the performances of the algorithm in segmenting the meaningful objects, in particular in detecting the lesion region by distinguishing it from the skin. Similarly to [1], we compare the performances of the algorithm with the segmentations obtained by using the Normalized Cut approach, adopted in some contexts for medical image segmentation [9, 14, 25, 3]. In particular, we choose the algorithm of Maji et al. [13] (*Biased NCut*) as the representative, in the following referred as *C-NCut*, because it is a Normalized Cut based algorithm for color-texture images. We observe that both *C-GeNCut* and *C-NCut*, are segmentation techniques for general kinds of images based on brightness, color and texture. Consequently, our goal is to assess which of the two kinds of approaches is more apt in segmenting skin lesion images.

The skin lesion images employed for the experimentation have been downloaded from DermAtlas[1], an open access web site with dermatological images, hosted by Johns Hopkins

[1]http://dermatlas.med.jhmi.edu

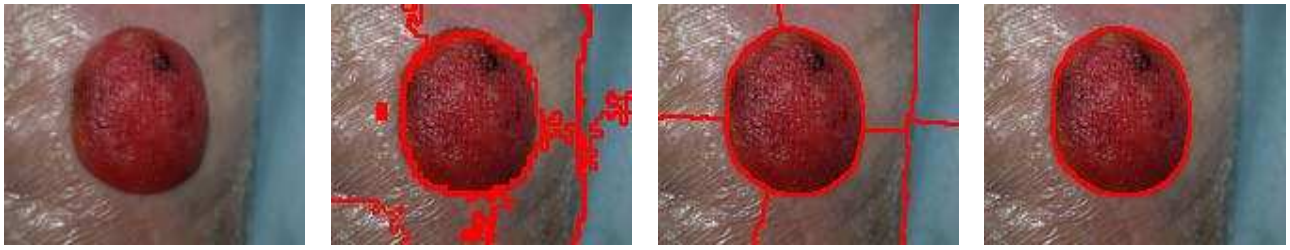

(a) (b) (c) (d)

Figure 1: Segmentation on a melanoma image. (a) is the original image, (b) is the *C-GeNCut* segmentation result, (c) is the *C-NCut* segmentation result by fixing the same number of segments as *C-GeNCut*, $k = 7$ and (d) is the *C-NCut* segmentation result with $k = 2$.

(a) (b) (c) (d)

Figure 2: Segmentation on a melanoma image. (a) is the original image, (b) is the *C-GeNCut* segmentation result, (c) is the *C-NCut* segmentation result by fixing the same number of segments as *C-GeNCut*, $k = 5$ and (d) is the *C-NCut* segmentation result with $k = 2$.

(a) (b) (c) (d)

Figure 3: Segmentation on a melanoma image. (a) is the original image, (b) is the *C-GeNCut* segmentation result, (c) is the *C-NCut* segmentation result by fixing the same number of segments as *C-GeNCut*, $k = 5$ and (d) is the *C-NCut* segmentation result with $k = 2$.

(a) (b) (c) (d)

Figure 4: Segmentation on a melanoma image. (a) is the original image, (b) is the *C-GeNCut* segmentation result, (c) is the *C-NCut* segmentation result by fixing the same number of segments as *C-GeNCut*, $k = 10$ and (d) is the *C-NCut* segmentation result with $k = 2$.

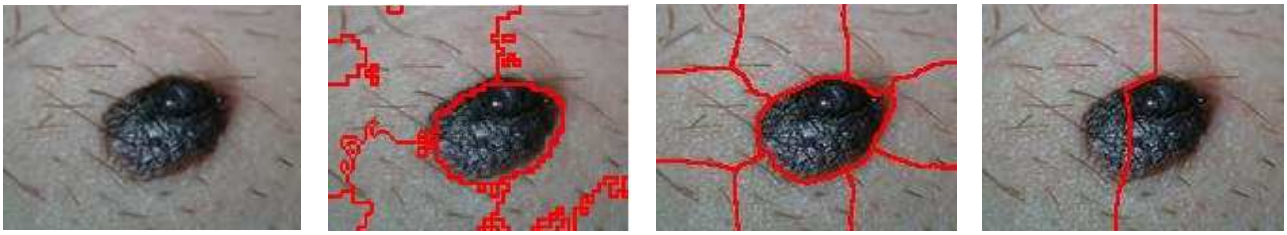

(a) (b) (c) (d)

Figure 5: Segmentation on a melanoma image. (a) is the original image, (b) is the *C-GeNCut* segmentation result, (c) is the *C-NCut* segmentation result by fixing the same number of segments as *C-GeNCut*, $k = 9$ and (d) is the *C-NCut* segmentation result with $k = 2$.

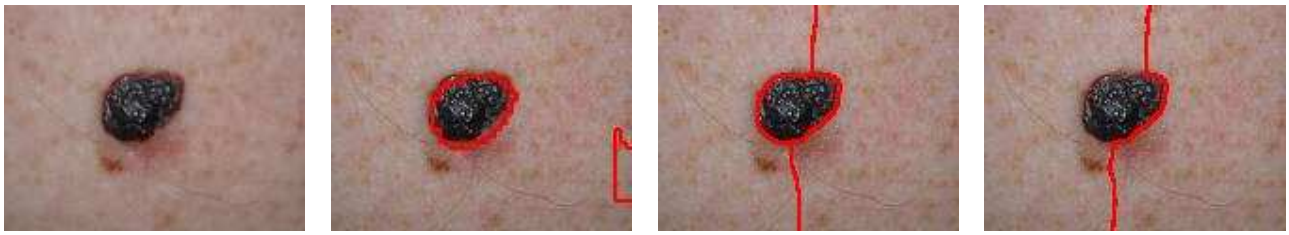

(a) (b) (c) (d)

Figure 6: Segmentation on a melanoma image. (a) is the original image, (b) is the *C-GeNCut* segmentation result, (c) is the *C-NCut* segmentation result by fixing the same number of segments as *C-GeNCut*, $k = 3$ and (d) is the *C-NCut* segmentation result with $k = 2$.

University's Dr. Bernard A. Cohen and Dr. Christoph U. Lehmann.

The version of the *Biased NCut* software is written in MATLAB and it is available at http://ttic.uchicago.edu/smaji/projects/biasedNcuts/. However we eliminated the interactive mode from the available algorithm specifically for performing comparisons with *C-GeNCut*.

The weight matrix of each image has been computed in the same way for both *C-NCut* and *C-GeNCut* methods, and it is based on the Intervening Contour framework that uses the multiscale *Pb* detector. We fix the same parameter values as in [1], which are $r = 5$ and $\rho = 0.1$. Recall that, about the *Pb* detector, the parameter σ, which defines the scales, is 5 pixels for the brightness channel, while for color and texture channels σ is 10 pixels. The parameters $\alpha_{i,s}$ are $0.01, 0.01, 0.02$ $0.02, 0.02, 0.03, 0.02, 0.02, 0.02, 0.01, 0.01$ and 0.01.

Since *C-NCut* needs the number k of clusters, we executed the algorithm by fixing the number k of segments to the same number of clusters found by *C-GeNCut*, and with $k = 2$ which is the best parameter value to detect the lesion region.

As regards *C-GeNCut* parameters, we set crossover rate to 0.9, mutation rate to 0.2, elite reproduction 10% of the population size, roulette selection function. The population size was 100, the number of generations 80.

In the following, for each image, we compare the segmentation results of *C-GeNCut* and *C-NCut* by depicting the contours of the regions obtained by the two approaches. For a more clear visualization, we show four images for each skin lesion image. The first image is the original image, the second one reports the boundary lines (in red) of the segmentation obtained by *C-GeNCut* on the original color image, the third image delineates the contours obtained by *C-NCut* (in red) on the original color image with k equal to the same number of segments found from *C-GeNCut*, the fourth image represents the contours obtained by *C-NCut* with $k = 2$.

First of all, we compare *C-GeNCut* and *C-NCut* on the melanoma images (Figures (1-6)). In Figure 1(a), representing a red nodular melanoma on a leg, the regions contours are detected from both *C-GeNCut* (Figure 1(b)) and *C-NCut* (Figure 1(c)). Furthermore, *C-NCut* perfectly delineates melanoma contour when the number of segments is fixed to 2 (Figure 1(d)).

Figure 2 is a red and purple gelatinous nodular melanoma on a leg. We observe as *C-GeNCut* performs a more precise segmentation of the lesion (Figure 2 (b)) than *C-NCut* which excludes the top left portion of the melanoma from the lesion region (Figure 2 (c)). When $k = 2$, *C-NCut* erroneously divides the image in two parts, of which the left segment contains the melanoma and the remaining left part of the skin.

Figure 3 illustrates a thick melanoma on an arm with smaller surrounding metastatic tumor nodules. Although *C-GeNCut* is not able to discriminate the melanoma from the surrounding nodules, it better circumscribes the region where both the lesions are located (Figure 3(b)), while *C-NCut* improperly includes the skin at the top side of the lesion region (Figure 3(c)). Also in this case the 2-segmentation is not able to isolate the tumor (Figure 3(d)).

In Figure 4, representing an ulcerated black melanoma arising of a brown slightly elevated plaque, both *C-GeNCut* and *C-NCut* are able to capture the melanoma area.

However, *C-GeNCut* segments the plaque together with the melanoma (Figure 4 (b)), while *C-NCut* separates the plaque from the melanoma, including the plaque into a healthy

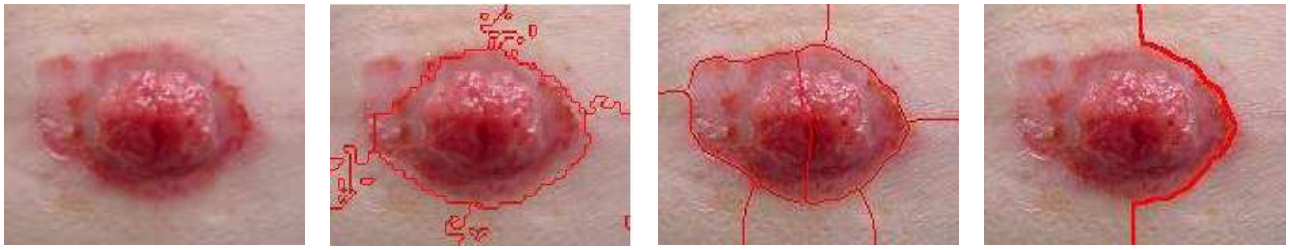

(a) (b) (c) (d)

Figure 7: Segmentation on a carcinoma image. (a) is the original image, (b) is the *C-GeNCut* segmentation result, (c) is the *C-NCut* segmentation result by fixing the same number of segments as *C-GeNCut*, $k = 7$ and (d) is the *C-NCut* segmentation result with $k = 2$.

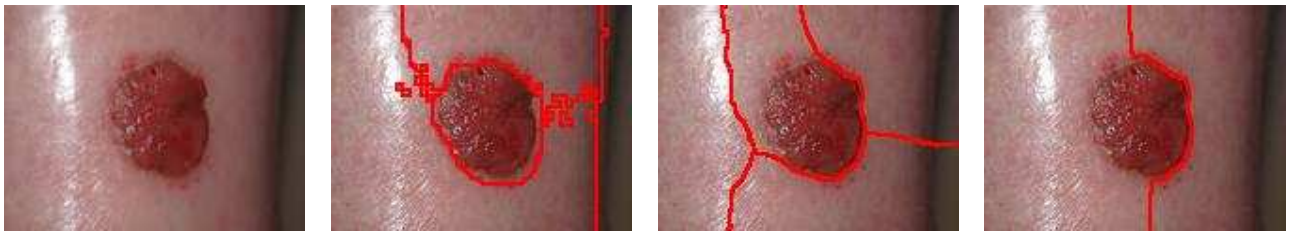

(a) (b) (c) (d)

Figure 8: Segmentation on a carcinoma image. (a) is the original image, (b) is the *C-GeNCut* segmentation result, (c) is the *C-NCut* segmentation result by fixing the same number of segments as *C-GeNCut*, $k = 4$ and (d) is the *C-NCut* segmentation result with $k = 2$.

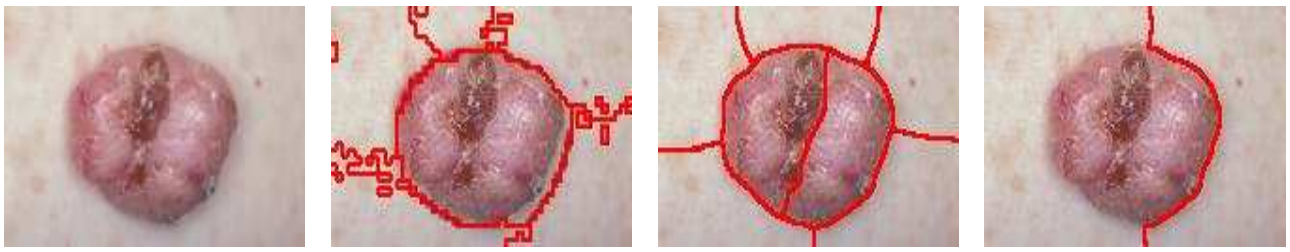

(a) (b) (c) (d)

Figure 9: Segmentation on a fibroepithelioma image. (a) is the original image, (b) is the *C-GeNCut* segmentation result, (c) is the *C-NCut* segmentation result by fixing the same number of segments as *C-GeNCut*, $k = 7$ and (d) is the *C-NCut* segmentation result with $k = 2$.

(a) (b) (c) (d)

Figure 10: Segmentation on a hemangioma image. (a) is the original image, (b) is the *C-GeNCut* segmentation result, (c) is the *C-NCut* segmentation result by fixing the same number of segments as *C-GeNCut*, $k = 13$ and (d) is the *C-NCut* segmentation result with $k = 2$.

skin region (Figure 4(c)). Figure 4(d) shows that *C-NCut* separates the image in two parts, completely disregarding the melanoma.

Figures 5, 6 are two brown papules representing, respectively, a melanoma on a chest and a melanoma on an arm. Both *C-GeNCut* and *C-NCut* properly discriminate the lesions region in both the images, in Figure 5(b), Figure 6(b) for *C-GeNCut* and in Figure 5(c), Figure 6(c) for *C-NCut* respectively. An incorrect division of the image can be seen in Figures 5(d) and 6(d).

The next images we consider for evaluation (Figures (7-10)) regard skin tumor, different from melanoma. Figures 7 and 8 depict a friable red gelatinous carcinoma on an abdomen and a leg, respectively, while Figure 9 is a red enlarging fibroepithelioma of Pincuson on a chest. For two images, *C-NCut* over-segments the skin lesion (Figure 7 (c), Figure 9 (c)), and fails in depicting the tumor border (Figure 7 (d), Figure 8 (d), Figure 9 (d)), while *C-GeNCut* depicts quite well the contours (Figure 7 (b), Figure 8 (b), Figure 9 (b)). In particular, we can observe that *C-GeNCut* captures the right shape of the tumor in Figure 8 (b), while *C-NCut* incorrectly includes the skin on the top side of the lesion segment (Figure 8 (c)).

Figure 10 is a red hemangioma appeared on a left labia. In such a case segmentation results of *C-GeNCut* and *C-NCut* are quite comparable. Although *C-NCut* is more precise than *C-GeNCut* in segmenting the lesion region (Figure 10 (c)), *C-GeNCut* behaves promising in discriminating the lesion from the rest of the skin (Figure 10 (b)). However, for $k = 2$, *C-NCut* again divides the image in two parts, one containing the lesion, but also the background skin (Figure 10)(d)). To conclude, though *C-GeNCut* generates an over-segmentation of the healthy skin, it is able to detect quite accurately the borders of skin lesion, thus a post processing phase that isolates tumor while merging the surrounding region could produce a promising and reliable lesion border detector.

4. CONCLUSIONS

The paper presented the application of a color image segmentation algorithm based on Genetic Algorithms for the segmentation of skin lesion images with the aim of detecting skin cancer. Experiments on different dermatological images showed the good performance of the approach, also when compared with another color image segmentation method. Future work aims at extending the segmentation algorithm for an accurate skin lesion detector, by including an appropriate region merging approach to isolate the lesions from the whole image background.

5. ACKNOWLEDGMENTS

This work has been partially supported by the project *MERIT : MEdical Research in Italy*, funded by MIUR.

6. REFERENCES

[1] A. Amelio and C. Pizzuti. A genetic algorithm for color image segmentation. In *16th European Conference on Applications of Evolutionary Computation, EvoApplications 2013*, pages 314–323, 2013.

[2] P. Arbelaez, M. Maire, C. Fowlkes, and J. Malik. Contour detection and hierarchical image segmentation. *IEEE Transactions on Pattern Anal. Mach. Intell.*, 33(5):898–916, May 2011.

[3] J. Carballido-gamio, S. J. Belongie, and S. Majumdar. Normalized cuts in 3-d for spinal mri segmentation. *IEEE Trans Med Imaging*, 23:36–44, 2004.

[4] M. E. Celebi, W. V. Stoecker, and R. H. Moss. Advances in skin cancer image analysis. *Computerized Medical Imaging and Graphics*, 35(2):83–84, 2011.

[5] T. Cour, F. Bénézit, and J. Shi. Spectral segmentation with multiscale graph decomposition. In *IEEE Computer Society Conference on Computer Vision and Pattern Recognition (CVPR 2005))*, pages 1124–1131, 2005.

[6] T. Donadey, C. Serruys, A. Giron, G. Aitken, J.-P. Vignali, R. Trille, and B. Fertil. Boundary detection of black skin tumors using an adaptive radial-based approach. In *Proc. SPIE 3979, Medical Imaging 2000: Image Processing*, pages 810–816, 2000.

[7] C. Fowlkes and J. Malik. How much does globalization help segmentation. Technical report, 2004.

[8] C. Fowlkes, D. Martin, and J. Malik. Learning Affinity Functions for Image Segmentation: Combining Patch-based and Gradient-based Approaches. *Computer Vision and Pattern Recognition, IEEE Computer Society Conference on*, 2, 2003.

[9] B. A. Goudannavar, R. S.Hegadi, and N. Patil. Hummers radiograph image segmentation using normalized cut. In *MPGI National Multi Conference 2012 (MPGINMC-2012)*, 2012.

[10] K. Korotkov and R. Garcia. Computerized analysis of pigmented skin lesions: a review. *Artificial Intelligence in Medicine*, 56:69–90, 2012.

[11] T. K. Leung and J. Malik. Contour continuity in region based image segmentation. In *5th European Conference on Computer Vision, ECCV'98*, pages 544–559, 1998.

[12] Z. Liu, J. Sun, M. Smith, L. Smith, and R. Warr. Unsupervised sub-segmentation for pigmented skin lesions. *Skin Research and Technology*, 18(1):77–87, 2012.

[13] S. Maji, N. K. Vishnoi, and J. Malik. Biased normalized cuts. In *CVPR*, pages 2057–2064. IEEE, 2011.

[14] S. Mandal, A. Kumar, J. Chatterjee, M. Manjunatha, and A. K. Ray. Segmentation of blood smear images using normalized cuts for detection of malarial parasites. In *India Conference (INDICON), 2010 Annual IEEE*, pages 1–4, 2010.

[15] M. Mete, S. Kockara, and K. Aydin. Fast density-based lesion detection in dermoscopy images. *Computerized Medical Imaging and Graphics*, 35(2):128 – 136, 2011.

[16] Y. Park and M. Song. A genetic algorithm for clustering problems. In *Proc. of 3rd Annual Conference on Genetic Algorithms*, pages 2–9, 1989.

[17] G. Schaefer, M. Rajab, M. Celebi, and H. Iyatomi. Skin lesion segmentation using co-operative neural network edge detection and colour normalisation. In *9th International Conference on Information Technology and Applications in Biomedicine, (ITAB 2009)*, pages 1–4, 2009.

[18] P. Schmid. Segmentation of digitized dermatoscopic images by two-dimensional color clustering. *IEEE Transactions on Medical Imaging*, 18(2):164–71, 1999.

[19] J. Shi and J. Malik. Normalized cuts and image segmentation. *IEEE Transactions on Pattern Analysis and Machine Intelligence*, 22(8):888–905, 2000.

[20] P. Wighton, T. K. Lee, G. Mori, H. Lui, D. I. McLean, and M. Atkins. Conditional random fields and supervised learning in automated skin lesion diagnosis. *Journal of Biomedical Imaging*, 2011, 2011.

[21] X. Yuan, N. Situ, and G. Zouridakis. Automatic segmentation of skin lesion images using evolution strategies. *Biomedical Signal Processing and Control*, 3(3):220–228, 2008.

[22] M. Yuksel and M. Borlu. Accurate segmentation of dermoscopic images by image thresholding based on type-2 fuzzy logic. *Fuzzy Systems, IEEE Transactions on*, 17(4):976–982, 2009.

[23] H. Zhou, G. Schaefer, M. E. Celebi, F. Lin, and T. Liu. Gradient vector flow with mean shift for skin lesion segmentation. *Computerized Medical Image and Graphics*, pages 121–127, 2011.

[24] H. Zhou, G. Schaefer, A. H. Sadka, and M. E. Celebi. Anisotropic mean shift based fuzzy c-means segmentation of dermoscopy images. *J. Sel. Topics Signal Processing*, pages 26–34, 2009.

[25] Y. Zhou, M. Smith, L. Smith, and R. Warr. Segmentation of clinical lesion images using normalized cut. In *10th Workshop on Image Analysis for Multimedia Interactive Services (WIAMIS '09)*, pages 101–104, 2009.